Letter

Quantum topological phase transitions in skyrmion crystals

Kristian Mæland and Asle Sudbø[*]
Center for Quantum Spintronics, Department of Physics, Norwegian University of Science and Technology, NO-7491 Trondheim, Norway

(Received 23 May 2022; accepted 29 June 2022; published 12 August 2022)

Topological order is important in many aspects of condensed matter physics and has been extended to bosonic systems. In this Letter we report on the nontrivial topology of the magnon bands in two distinct quantum skyrmion crystals appearing in zero external magnetic field. This is revealed by nonzero Chern numbers for some of the bands. As a bosonic analog of the quantum anomalous Hall effect, we show that topological magnons can appear in skyrmion crystals without explicitly breaking time-reversal symmetry with an external magnetic field. By tuning the value of the easy-axis anisotropy at zero temperature, we find eight quantum topological phase transitions signaled by discontinuous jumps in certain Chern numbers. We connect these quantum topological phase transitions to gaps closing and reopening between magnon bands.

DOI: 10.1103/PhysRevResearch.4.L032025

Introduction. Topological order in fermionic condensed matter systems lies at the heart of the understanding of the quantum Hall effect (QHE) [1,2], the quantum anomalous Hall effect (QAHE) [3,4], the quantum spin Hall effect (QSHE) [5], and topological insulators (TIs) [6]. The QHE involves explicit time-reversal symmetry breaking by an external magnetic field, while the QSHE and TIs are found in time-reversal-symmetric systems [5–8]. The QAHE is a special case, taking place in systems where time-reversal symmetry is spontaneously, and not explicitly, broken. It is thus a manifestation of the QHE without the need for an external magnetic field [4]. It was later shown that also bosonic excitations may feature topological properties [9–12]. The collective fluctuations of quantum spins, i.e., magnons, have been shown to be topologically nontrivial in magnonic crystals [9], dipolar magnetic thin films [10], and in ferromagnets on the honeycomb lattice [13–17]. In the model used in Refs. [13–15], next-nearest neighbor Dzyaloshinskii-Moriya interaction (DMI) realizes a bosonic analog of the Haldane model [3] in a system of insulating spins.

Even though analogies were proposed [13,17–20], topological magnon systems do not show direct equivalences of the QHE, QAHE, and QSHE [5,6,15]. Since bosons obey Bose-Einstein rather than Fermi-Dirac statistics, the Hall conductivity is not quantized [15]. The authors of Ref. [11] introduced the bosonic analog of a TI, a topological magnon insulator. The nontrivial topology of the magnon bands gives rise to chiral edge states within a bulk magnon gap. However, since bosonic systems lack the concept of a Fermi surface, the bulk is not guaranteed to be insulating with respect to spin currents [14]. Still, the chiral edge states resulting from topologically nontrivial magnons allow the creation of magnon currents that are insensitive to backscattering and disorder [9,10]. These hold promising applications such as spin-current splitters, waveguides, and interferometers [9,12]. In addition, magnetoelastic coupling leads to chiral phonon transport induced by the topological magnons [15].

The nontrivial real-space magnetic texture of skyrmions means they are topologically protected [21,22]. Therefore, skyrmions received a great deal of interest, and are being explored for applications in magnetic memory technology, unconventional computing, and numerous other applications [22–35]. The reciprocal space topology held by the magnon bands in skyrmion crystals (SkXs) was also explored [36–40], and a topological phase transition driven by a magnetic field was found in Ref. [38]. Furthermore, evidence of the nontrivial topology of magnon bands in SkXs was observed in an experiment [40].

In Ref. [41], we explored the quantum fluctuations of the order parameter for quantum SkXs. Quantum skyrmions are skyrmions with such a small size that the continuum limit breaks down and the quantum nature of the individual spins is not negligible [41–43]. In this Letter we reveal eight quantum topological phase transitions (QTPTs) [7,44–46] driven by a tunable easy-axis anisotropy in the same quantum SkXs that are explored in Ref. [41]. These QTPTs are signaled by discontinuous jumps in the Chern numbers [9] of the magnon bands. Here, we consider QTPTs to be topological phase transitions occurring at zero temperature by tuning a parameter in the Hamiltonian. The SkXs we consider are inspired by the observation of a SkX containing nanometer-sized skyrmions in a magnetic monolayer [47]. Since the SkXs are stabilized in zero external magnetic field [41,47], the QTPTs occur in a time-reversal-symmetric model. Instead, the magnetic order of the SkX ground state (GS) spontaneously breaks time-reversal symmetry, allowing nonzero Chern numbers [12]. In that sense, our skyrmion system is analogous to the QAHE in fermionic systems. This is in contrast to previous studies of

[*]Corresponding author: asle.sudbo@ntnu.no

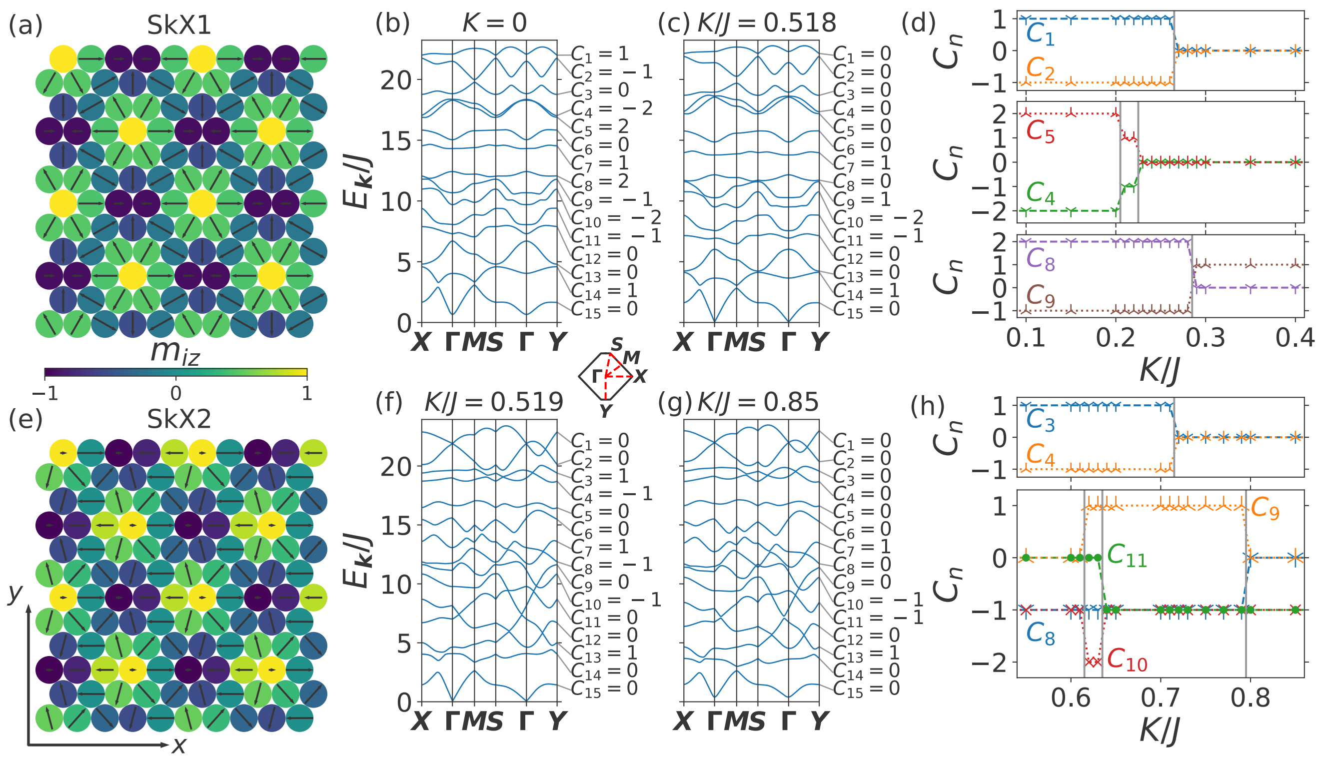

FIG. 1. (a) The classical ground state of the skyrmion crystal SkX1, (b) its magnon spectrum at low K along with the Chern numbers of each band, and (c) its magnon spectrum at high K along with the Chern numbers of each band. In (a), colors indicate the z component of the unit vector determining the direction of the spin m_{iz}, while arrows show its projection on the xy plane. The spectra are plotted along the path in the first Brillouin zone (1BZ) that is sketched in the middle. (d) Shows the four quantum topological phase transitions (QTPTs) found in SkX1, where some Chern numbers show discontinuous jumps at the approximate values of K/J shown in gray. The calculated Chern numbers are shown with markers, while dotted or dashed lines are included for illustration. (e)–(h) The same as (a)–(d), but for the distinct skyrmion crystal SkX2. The parameters are $D/J = 2.16$, $U/J = 0.35$, $S = 1$, (a) $K/J = 0.518$, and (e) $K/J = 0.519$.

topological magnons in SkXs, where time-reversal symmetry is explicitly broken by external magnetic fields [36–40].

As pointed out in Ref. [37], the bulk-edge correspondence is not guaranteed unless the finite geometry contains an integer number of unit cells. However, by letting the GS adapt to a strip geometry, the authors of Refs. [36–38] found the expected number and chirality [9] of edge states based on the bulk Chern numbers in SkXs. Therefore, we will not explicitly prove the existence of chiral edge states here. Assuming the validity of the bulk-edge correspondence in a finite geometry, the QTPTs could be used to switch chiral edge states on and off.

Model. As in Ref. [41], we use the time-reversal-symmetric Hamiltonian

$$H = H_{\text{ex}} + H_{\text{DM}} + H_{\text{A}} + H_4, \tag{1}$$

where

$$H_{\text{ex}} = -J \sum_{\langle ij \rangle} \boldsymbol{S}_i \cdot \boldsymbol{S}_j, \tag{2}$$

$$H_{\text{DM}} = \sum_{\langle ij \rangle} \boldsymbol{D}_{ij} \cdot (\boldsymbol{S}_i \times \boldsymbol{S}_j), \tag{3}$$

$$H_{\text{A}} = -K \sum_i S_{iz}^2, \tag{4}$$

$$H_4 = U \sum_{ijkl}^{\diamond} [(\boldsymbol{S}_i \cdot \boldsymbol{S}_j)(\boldsymbol{S}_k \cdot \boldsymbol{S}_l) + (\boldsymbol{S}_i \cdot \boldsymbol{S}_l)(\boldsymbol{S}_j \cdot \boldsymbol{S}_k) - (\boldsymbol{S}_i \cdot \boldsymbol{S}_k)(\boldsymbol{S}_j \cdot \boldsymbol{S}_l)]. \tag{5}$$

The spin operator $\boldsymbol{S}_i$, with magnitude S, pertains to lattice site i on the triangular lattice. We consider a nearest-neighbor ferromagnetic exchange interaction, $J > 0$. In Ref. [47], the DMI between Fe atoms on the surface originates with the strong spin-orbit coupling from the Ir atoms [23]. We assume a similar effect in our model and set the DMI vector to $\boldsymbol{D}_{ij} = D\hat{r}_{ij} \times \hat{z}$, where $\hat{r}_{ij}$ is a unit vector from site i to site j. Like in Ref. [41], we will discuss a tunable easy-axis anisotropy K, motivated by the findings of Refs. [48,49] where it was shown that applying mechanical strain can tune the magnetic anisotropy. The Hamiltonian also contains the four-spin interaction H_4, acting between four sites that are oriented counterclockwise and make diamonds of minimal area [47,50]. The reduced Planck's constant $\hbar$ and the lattice constant a are set to 1.

We refer to Refs. [41,51] for details of the two distinct SkX GSs, which are separated by a quantum phase transition (QPT) at $K = K_t$ with $K_t/J \in (0.518, 0.519)$. The classical GSs of SkX1 and SkX2 are shown in Figs. 1(a) and 1(e) for $K/J = 0.518$ and $K/J = 0.519$, respectively. By including quantum corrections in a calculation of the expectation value of the Hamiltonian, it is found that $\langle H \rangle$ is lower than the classical GS energy. Hence, quantum skyrmions are energetically preferred over their corresponding classical GSs [41,51]. The introduction of the Holstein-Primakoff transformation via rotated coordinates [52] involves approximations whose validity are discussed in Refs. [41,51]. Possible corrections to our predictions due to the ignored magnon-magnon interactions are discussed in Refs. [12,37]. Dipolar interactions were shown to affect the high-energy magnon bands of SkXs in Ref. [39]. Since we consider a magnetic monolayer, dipolar interactions are not expected to have significant effects [23,47]. The study of dipolar interactions is also beyond the scope of this Letter. For these reasons, they are excluded from our model.

The diagonalization of the system to obtain the magnon bands [53] is shown in detail in Refs. [41,51]. We take the transformation matrices $T_{\boldsymbol{k}}$ and the magnon bands $E_{\boldsymbol{k},n}$ as inputs in this Letter. The 15 magnon bands are numbered from top to bottom in terms of energy. The first Brillouin zone (1BZ) is the same for all 15 sublattices in both SkX1 and SkX2 and we define the points $\boldsymbol{\Gamma} = (0, 0)$, $\boldsymbol{X} = (52\pi/135, 0)$, $\boldsymbol{M} = (\pi/5, \pi/3\sqrt{3})$, $\boldsymbol{S} = (2\pi/135, 2\pi/3\sqrt{3})$, and $\boldsymbol{Y} = (0, -2\pi/3\sqrt{3})$ in the 1BZ [41,51]. These points and the 1BZ are sketched in Fig. 1.

Chern numbers. Let Γ_n be a matrix whose nth diagonal element is 1 and all other matrix elements are zero, $\Gamma_{n,i,j} = \delta_{in}\delta_{jn}$. From this, we define a projection matrix $P_{\boldsymbol{k},n} = T_{\boldsymbol{k}}^{-1}\Gamma_n T_{\boldsymbol{k}}$. The bosonic nature of the magnons is encoded in the paraunitary transformation matrix [41,51,53]. Then the Berry curvature of the nth band is given by [2,9]

$$B_n(\boldsymbol{k}) = i\epsilon_{\mu\nu}\mathrm{Tr}\big[\big(\delta_{k_\mu}P_{\boldsymbol{k},n}\big)P_{\boldsymbol{k},n}\big(\delta_{k_\nu}P_{\boldsymbol{k},n}\big)\big], \tag{6}$$

where $\epsilon_{\mu\nu}$ is the Levi-Civita tensor and $\mu, \nu \in \{x, y\}$. The Chern number of the nth band is its Berry curvature integrated over the 1BZ

$$C_n = \frac{1}{2\pi}\int_{1\mathrm{BZ}} d\boldsymbol{k} B_n(\boldsymbol{k}). \tag{7}$$

It can be shown that the Chern numbers are integers, given that the bands are isolated [9]. Here, we calculate the Chern numbers using numerical approximations to the integral. We consider equally spaced discretizations and adaptive quadratures [51,54]. When the numerical results are found to approach integers upon increasing the density of $\boldsymbol{k}$ points, we present the Chern numbers as integers.

Quantum topological phase transitions. In Figs. 1(b) and 1(c) we show the magnon spectrum in SkX1 for $K = 0$ and for $K/J = 0.518$, i.e., close to the QPT to SkX2. The Chern numbers of the 15 bands are given at both values of K and it is clear that some of them have changed due to the change in easy-axis anisotropy. In Fig. 1(d) we plot these as a function of K, revealing four QTPTs. $E_{\boldsymbol{k},4}$ and $E_{\boldsymbol{k},5}$ first cross at the $\boldsymbol{Y}$ point for the specific value $K = K_1$, where K_1/J is in the interval (0.20, 0.21). They also cross at the $\boldsymbol{\Gamma}$ point for $K/J = K_2/J \in (0.22, 0.23)$. The gap between the bands closes and reopens, and their Chern numbers change, signaling QTPTs. $E_{\boldsymbol{k},1}$ and $E_{\boldsymbol{k},2}$ cross at the $\boldsymbol{Y}$ point for $K/J = K_3/J \in (0.26, 0.27)$. The two Chern numbers annihilate, and both bands are topologically trivial for $K > K_3$. Finally, the gap between $E_{\boldsymbol{k},8}$ and $E_{\boldsymbol{k},9}$ closes between the $\boldsymbol{\Gamma}$ point and the $\boldsymbol{X}$ point for $K/J = K_4/J \in (0.28, 0.29)$. Only $E_{\boldsymbol{k},9}$ remains topologically nontrivial when the gap reopens for $K > K_4$. In SkX1, the magnon band with lowest energy is topologically trivial, while the band with second lowest energy is topologically nontrivial. For ferromagnetic SkXs in an external magnetic field, the band with third lowest energy is topologically nontrivial while the two bands with lower energy are topologically trivial [36,38–40].

Figures 1(e) and 1(f) show the magnon spectrum in SkX2 for $K/J = 0.519$ and $K/J = 0.85$. Despite the plethora of closely avoided crossings, all the bands are isolated at these values of K, and all 15 Chern numbers are well defined. Notice that in all cases the sum of the Chern numbers of all bands is zero, as expected [9]. It is clear that the Chern numbers have changed from the spectrum of SkX1 at $K/J = 0.518$ to the spectrum of SkX2 at $K/J = 0.519$. We do not view this as a QTPT since it is not due to gaps closing and reopening in the magnon spectrum. Rather, the magnon spectra are different from the outset since they arise from two distinct SkXs.

In Fig. 1(g) we plot the Chern numbers that change when tuning K in SkX2. We find four QTPTs. The gap between $E_{\boldsymbol{k},9}$ and $E_{\boldsymbol{k},10}$ closes between $\boldsymbol{\Gamma}$ and $\boldsymbol{Y}$ for $K/J = K_5/J \in (0.61, 0.62)$. Once the gap reopens, $E_{\boldsymbol{k},9}$ has become topologically nontrivial, while $C_{10} = -1$ has jumped to $C_{10} = -2$. $E_{\boldsymbol{k},10}$ and $E_{\boldsymbol{k},11}$ cross between $\boldsymbol{\Gamma}$ and $\boldsymbol{Y}$ for $K/J = K_6/J \in (0.63, 0.64)$. C_{10} jumps back to -1, allowing $E_{\boldsymbol{k},11}$ to become topologically nontrivial for $K > K_6$. The gap between $E_{\boldsymbol{k},3}$ and $E_{\boldsymbol{k},4}$ closes between $\boldsymbol{\Gamma}$ and $\boldsymbol{Y}$ for $K/J = K_7/J \in (0.71, 0.72)$. Once the gap reopens at $K > K_7$ they are both topologically trivial. Finally, $E_{\boldsymbol{k},8}$ and $E_{\boldsymbol{k},9}$ cross at $\boldsymbol{k} \approx (\pm 0.32, 0.10)$ for $K/J = K_8/J \in (0.79, 0.80)$ and are left topologically trivial for $K > K_8$.

Gap closing and Berry curvature. In Fig. 2(a) we go into detail of the two band crossings of $E_{\boldsymbol{k},4}$ and $E_{\boldsymbol{k},5}$ in SkX1. For $K < K_1$ we have $C_4 = -2, C_5 = 2$. Then, at $K = K_1$ the gap between $E_{\boldsymbol{k},4}$ and $E_{\boldsymbol{k},5}$ at the $\boldsymbol{Y}$ point closes, $\Delta_{4,5}^{\boldsymbol{Y}} = 0$, and the two Chern numbers are undefined [9]. For $K > K_1$ the gap reopens and $C_4 = -1, C_5 = 1$, i.e., the bands remain topologically nontrivial. For $K = K_2$ the gap closes at the $\boldsymbol{\Gamma}$ point $\Delta_{4,5}^{\boldsymbol{\Gamma}} = 0$. When the gap reopens for $K > K_2$ both bands have become topologically trivial. The dependence of these two gaps on the easy-axis anisotropy is shown in Fig. 2(b). It appears the two gaps close with an approximately linear dependence on K.

The Berry curvatures of $E_{\boldsymbol{k},4}$ and $E_{\boldsymbol{k},5}$ are shown in Fig. 2(c). At $K = 0$, $B_4(\boldsymbol{k})$ has extended negative valleys, giving rise to a negative Chern number. For $K/J = 0.22$, $\Delta_{4,5}^{\boldsymbol{\Gamma}}$ is small and so there is a sharp negative valley in $B_4(\boldsymbol{k})$ around $\boldsymbol{k} = \boldsymbol{\Gamma}$. Again, this gives rise to a negative Chern number. At $K/J = 0.3$, the Berry curvature contains both positive peaks and negative valleys, which cancel each other out in the integral and lead to zero Chern number. The arguments are similar for $B_5(\boldsymbol{k})$ and C_5. From these figures, it is clear that the gap closings involve an exchange of Berry curvature between the bands. Also, the Berry curvature of a given band has its largest absolute values where the band has the smallest gap to neighboring bands. Similar figures and arguments can be extended to the remaining six QTPTs discussed in this Letter. Notice that each time two bands cross and undergo a QTPT, the sum of their Chern numbers is preserved, as expected [2].

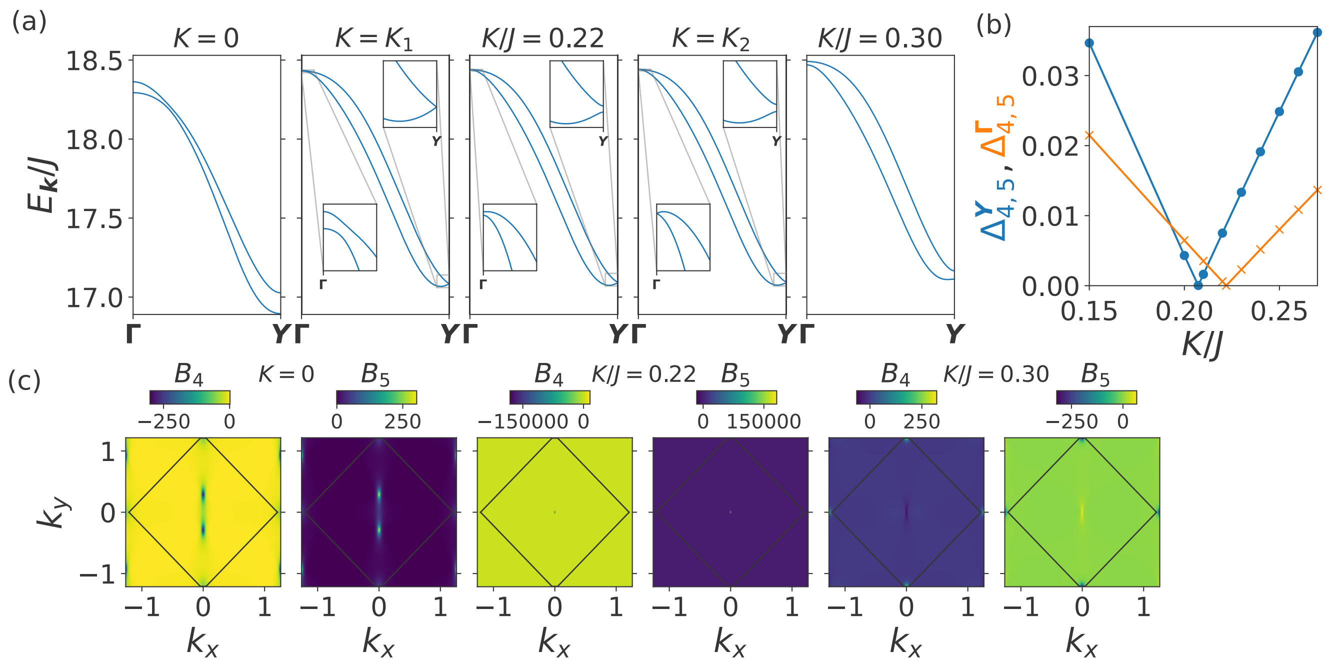

FIG. 2. (a) Plots of $E_{\boldsymbol{k},4}$ and $E_{\boldsymbol{k},5}$ in SkX1 at varying K showing how the gap at $\boldsymbol{Y}$ closes at $K = K_1$ where there is a QTPT, and $C_4 = -2, C_5 = 2$ at $K < K_1$ goes to $C_4 = -1, C_5 = 1$ at $K_1 < K < K_2$ once the gap reopens. Also, the gap closes at the $\boldsymbol{\Gamma}$ point for $K = K_2$, and once it reopens, the two bands are topologically trivial. (b) The gap between $E_{\boldsymbol{k},4}$ and $E_{\boldsymbol{k},5}$ at the $\boldsymbol{Y}$ ($\boldsymbol{\Gamma}$) point is shown in blue (orange), with circles (crosses) at the calculated values. (c) The Berry curvatures of bands $E_{\boldsymbol{k},4}$ and $E_{\boldsymbol{k},5}$ shown for the three values of K in (a) where the bands are isolated. The 1BZ is indicated in black and the Berry curvatures are plotted with 201 points in each direction. The parameters are $D/J = 2.16, U/J = 0.35$, and $S = 1$.

Predicted edge states. The predicted number of edge states within the gap between the bands $E_{\boldsymbol{k},n}$ and $E_{\boldsymbol{k},n+1}$ is

$$\nu_n = \sum_{n'=n+1}^{15} C_{n'}. \tag{8}$$

The chiral edge states propagate clockwise (counterclockwise) for positive (negative) ν_n [9]. For instance, we predict a clockwise edge state within the bulk band gap between $E_{\boldsymbol{k},13}$ and $E_{\boldsymbol{k},14}$ in SkX1. Let SkX3 be the result of applying the time-reversal operator, i.e., flipping all spins, to SkX1. In Ref. [41], we mentioned that since the Hamiltonian in Eq. (1) is time-reversal symmetric, SkX1 and SkX3 are degenerate in energy. It was also mentioned that the two states can appear concurrently, separated by domain walls. SkX3 has the same magnon spectrum as SkX1, while the Chern numbers change sign. At the interface between two topologically nontrivial systems A and B, with $\nu_n = \nu_A$ and $\nu_n = \nu_B$ in the same energy interval, one expects $|\nu_A - \nu_B|$ edge states [36]. Therefore, along a domain wall between SkX1 and SkX3, we predict two chiral edge states within the gap between $E_{\boldsymbol{k},13}$ and $E_{\boldsymbol{k},14}$.

Conclusion. We found eight quantum topological phase transitions in two distinct skyrmion crystals that are stabilized in a time-reversal-symmetric model. Time-reversal symmetry is spontaneously broken by the magnetic ordering of the skyrmions, and therefore nonzero Chern numbers of the magnon bands are possible. This is a bosonic analog of the quantum anomalous Hall effect. The quantum topological phase transitions, driven by a tunable easy-axis anisotropy at zero temperature, are signaled by jumps in the Chern numbers. We illustrated how the closing and subsequent reopening of the gaps between magnon bands leads to these jumps in the Chern numbers, and how the Berry curvature depends on these gaps.

Acknowledgments. We acknowledge funding from the Research Council of Norway through its Centres of Excellence funding scheme, Project No. 262633, "QuSpin," and through Project No. 323766, "Equilibrium and out-of-equilibrium quantum phenomena in superconducting hybrids with antiferromagnets and topological insulators."

[1] D. J. Thouless, M. Kohmoto, M. P. Nightingale, and M. den Nijs, Quantized Hall Conductance in a Two-Dimensional Periodic Potential, Phys. Rev. Lett. **49**, 405 (1982).

[2] J. E. Avron, R. Seiler, and B. Simon, Homotopy and Quantization in Condensed Matter Physics, Phys. Rev. Lett. **51**, 51 (1983).

[3] F. D. M. Haldane, Model for a Quantum Hall Effect without Landau Levels: Condensed-Matter Realization of the "Parity Anomaly", Phys. Rev. Lett. **61**, 2015 (1988).

[4] C.-X. Liu, S.-C. Zhang, and X.-L. Qi, The Quantum Anomalous Hall Effect: Theory and Experiment, Annu. Rev. Condens. Matter Phys. **7**, 301 (2016).

[5] C. L. Kane and E. J. Mele, Z_2 Topological Order and the Quantum Spin Hall Effect, Phys. Rev. Lett. **95**, 146802 (2005).

[6] M. Z. Hasan and C. L. Kane, *Colloquium:* Topological insulators, Rev. Mod. Phys. **82**, 3045 (2010).
[7] B. A. Bernevig, T. L. Hughes, and S.-C. Zhang, Quantum Spin Hall Effect and Topological Phase Transition in HgTe Quantum Wells, Science **314**, 1757 (2006).
[8] J. E. Moore and L. Balents, Topological invariants of time-reversal-invariant band structures, Phys. Rev. B **75**, 121306(R) (2007).
[9] R. Shindou, R. Matsumoto, S. Murakami, and J.-i. Ohe, Topological chiral magnonic edge mode in a magnonic crystal, Phys. Rev. B **87**, 174427 (2013).
[10] R. Shindou, J.-i. Ohe, R. Matsumoto, S. Murakami, and E. Saitoh, Chiral spin-wave edge modes in dipolar magnetic thin films, Phys. Rev. B **87**, 174402 (2013).
[11] L. Zhang, J. Ren, J.-S. Wang, and B. Li, Topological magnon insulator in insulating ferromagnet, Phys. Rev. B **87**, 144101 (2013).
[12] P. A. McClarty, Topological Magnons: A Review, Annu. Rev. Condens. Matter Phys. **13**, 171 (2022).
[13] S. K. Kim, H. Ochoa, R. Zarzuela, and Y. Tserkovnyak, Realization of the Haldane-Kane-Mele Model in a System of Localized Spins, Phys. Rev. Lett. **117**, 227201 (2016).
[14] A. Rückriegel, A. Brataas, and R. A. Duine, Bulk and edge spin transport in topological magnon insulators, Phys. Rev. B **97**, 081106(R) (2018).
[15] E. Thingstad, A. Kamra, A. Brataas, and A. Sudbø, Chiral Phonon Transport Induced by Topological Magnons, Phys. Rev. Lett. **122**, 107201 (2019).
[16] S. A. Owerre, A first theoretical realization of honeycomb topological magnon insulator, J. Phys.: Condens. Matter **28**, 386001 (2016).
[17] H. Huang, T. Kariyado, and X. Hu, Topological magnon modes on honeycomb lattice with coupling textures, Sci. Rep. **12**, 6257 (2022).
[18] K. Nakata, J. Klinovaja, and D. Loss, Magnonic quantum Hall effect and Wiedemann-Franz law, Phys. Rev. B **95**, 125429 (2017).
[19] K. H. Lee, S. B. Chung, K. Park, and J.-G. Park, Magnonic quantum spin Hall state in the zigzag and stripe phases of the antiferromagnetic honeycomb lattice, Phys. Rev. B **97**, 180401(R) (2018).
[20] S. A. Owerre, Floquet topological magnons, J. Phys. Commun. **1**, 021002 (2017).
[21] S.-G. Je, H.-S. Han, S. K. Kim, S. A. Montoya, W. Chao, I.-S. Hong, E. E. Fullerton, K.-S. Lee, K.-J. Lee, M.-Y. Im, and J.-I. Hong, Direct Demonstration of Topological Stability of Magnetic Skyrmions *via* Topology Manipulation, ACS Nano **14**, 3251 (2020).
[22] N. Nagaosa and Y. Tokura, Topological properties and dynamics of magnetic skyrmions, Nat. Nanotechnol. **8**, 899 (2013).
[23] G. Finocchio, F. Büttner, R. Tomasello, M. Carpentieri, and M. Kläui, Magnetic skyrmions: From fundamental to applications, J. Phys. D: Appl. Phys. **49**, 423001 (2016).
[24] F. Jonietz, S. Mühlbauer, C. Pfleiderer, A. Neubauer, W. Münzer, A. Bauer, T. Adams, R. Georgii, P. Böni, R. A. Duine, K. Everschor, M. Garst, and A. Rosch, Spin transfer torques in MnSi at ultralow current densities, Science **330**, 1648 (2010).
[25] C. Back, V. Cros, H. Ebert, K. Everschor-Sitte, A. Fert, M. Garst, T. Ma, S. Mankovsky, T. L. Monchesky, M. Mostovoy, N. Nagaosa, S. S. P. Parkin, C. Pfleiderer, N. Reyren, A. Rosch, Y. Taguchi, Y. Tokura, K. von Bergmann, and J. Zang, The 2020 skyrmionics roadmap, J. Phys. D: Appl. Phys. **53**, 363001 (2020).
[26] R. Tomasello, E. Martinez, R. Zivieri, L. Torres, M. Carpentieri, and G. Finocchio, A strategy for the design of skyrmion racetrack memories, Sci. Rep. **4**, 6784 (2015).
[27] A. Fert, V. Cros, and J. Sampaio, Skyrmions on the track, Nat. Nanotechnol. **8**, 152 (2013).
[28] V. V. Mazurenko, Y. O. Kvashnin, A. I. Lichtenstein, and M. I. Katsnelson, A DMI guide to magnets micro-world, J. Exp. Theor. Phys. **132**, 506 (2021).
[29] E. A. Stepanov, C. Dutreix, and M. I. Katsnelson, Dynamical and Reversible Control of Topological Spin Textures, Phys. Rev. Lett. **118**, 157201 (2017).
[30] E. A. Stepanov, S. A. Nikolaev, C. Dutreix, M. I. Katsnelson, and V. V. Mazurenko, Heisenberg-exchange-free nanoskyrmion mosaic, J. Phys.: Condens. Matter **31**, 17LT01 (2019).
[31] N. Romming, C. Hanneken, M. Menzel, J. E. Bickel, B. Wolter, K. von Bergmann, A. Kubetzka, and R. Wiesendanger, Writing and Deleting Single Magnetic Skyrmions, Science **341**, 636 (2013).
[32] P.-J. Hsu, A. Kubetzka, A. Finco, N. Romming, K. von Bergmann, and R. Wiesendanger, Electric-field-driven switching of individual magnetic skyrmions, Nat. Nanotechnol. **12**, 123 (2017).
[33] G. Yu, P. Upadhyaya, Q. Shao, H. Wu, G. Yin, X. Li, C. He, W. Jiang, X. Han, P. K. Amiri, and K. L. Wang, Room-temperature skyrmion shift device for memory application, Nano Lett. **17**, 261 (2017).
[34] X. Zhang, M. Ezawa, and Y. Zhou, Magnetic skyrmion logic gates: conversion, duplication and merging of skyrmions, Sci. Rep. **5**, 9400 (2015).
[35] C. Psaroudaki and C. Panagopoulos, Skyrmion Qubits: A New Class of Quantum Logic Elements Based on Nanoscale Magnetization, Phys. Rev. Lett. **127**, 067201 (2021).
[36] A. Roldán-Molina, A. S. Nunez, and J. Fernández-Rossier, Topological spin waves in the atomic-scale magnetic skyrmion crystal, New J. Phys. **18**, 045015 (2016).
[37] S. A. Díaz, J. Klinovaja, and D. Loss, Topological Magnons and Edge States in Antiferromagnetic Skyrmion Crystals, Phys. Rev. Lett. **122**, 187203 (2019).
[38] S. A. Díaz, T. Hirosawa, J. Klinovaja, and D. Loss, Chiral magnonic edge states in ferromagnetic skyrmion crystals controlled by magnetic fields, Phys. Rev. Research **2**, 013231 (2020).
[39] J. Waizner, Spin wave excitations in magnetic helices and skyrmion lattices, Ph.D. thesis, Universität zu Köln, 2016, http://kups.ub.uni-koeln.de/id/eprint/7937.
[40] T. Weber, D. M. Fobes, J. Waizner, P. Steffens, G. S. Tucker, M. Böhm, L. Beddrich, C. Franz, H. Gabold, R. Bewley, D. Voneshen, M. Skoulatos, R. Georgii, G. Ehlers, A. Bauer, C. Pfleiderer, P. Böni, M. Janoschek, and M. Garst, Topological magnon band structure of emergent Landau levels in a skyrmion lattice, Science **375**, 1025 (2022).
[41] K. Mæland and A. Sudbø, Quantum fluctuations in the order parameter of quantum skyrmion crystals, Phys. Rev. B **105**, 224416 (2022).
[42] O. M. Sotnikov, V. V. Mazurenko, J. Colbois, F. Mila, M. I. Katsnelson, and E. A. Stepanov, Probing the topology of the

quantum analog of a classical skyrmion, Phys. Rev. B **103**, L060404 (2021).

[43] V. Lohani, C. Hickey, J. Masell, and A. Rosch, Quantum Skyrmions in Frustrated Ferromagnets, Phys. Rev. X **9**, 041063 (2019).

[44] C. Castelnovo and C. Chamon, Quantum topological phase transition at the microscopic level, Phys. Rev. B **77**, 054433 (2008).

[45] A. Hamma, W. Zhang, S. Haas, and D. A. Lidar, Entanglement, fidelity, and topological entropy in a quantum phase transition to topological order, Phys. Rev. B **77**, 155111 (2008).

[46] E. Samimi, M. H. Zarei, and A. Montakhab, Global entanglement in a topological quantum phase transition, Phys. Rev. A **105**, 032438 (2022).

[47] S. Heinze, K. von Bergmann, M. Menzel, J. Brede, A. Kubetzka, R. Wiesendanger, G. Bihlmayer, and S. Blügel, Spontaneous atomic-scale magnetic skyrmion lattice in two dimensions, Nat. Phys. **7**, 713 (2011).

[48] L. Webster and J.-A. Yan, Strain-tunable magnetic anisotropy in monolayer $CrCl_3$, $CrBr_3$, and CrI_3, Phys. Rev. B **98**, 144411 (2018).

[49] R. Albaridy, A. Manchon, and U. Schwingenschlögl, Tunable magnetic anisotropy in Cr–trihalide Janus monolayers, J. Phys.: Condens. Matter **32**, 355702 (2020).

[50] A. H. MacDonald, S. M. Girvin, and D. Yoshioka, $\frac{t}{U}$ expansion for the Hubbard model, Phys. Rev. B **37**, 9753 (1988).

[51] See Supplemental Material at http://link.aps.org/supplemental/10.1103/PhysRevResearch.4.L032025 for (i) details regarding the ground states and how they were obtained, (ii) the introduction of the Holstein-Primakoff transformation through rotated coordinates and the Fourier transform of the magnon description, (iii) the diagonalization to obtain the magnon bands, and (iv) details of the Chern number calculation. The Supplemental Material contains Refs. [55–62].

[52] J. T. Haraldsen and R. S. Fishman, Spin rotation technique for non-collinear magnetic systems: application to the generalized Villain model, J. Phys.: Condens. Matter **21**, 216001 (2009).

[53] J. H. P. Colpa, Diagonalization of the quadratic boson Hamiltonian, Phys. A: Stat. Mech. Appl. **93**, 327 (1978).

[54] S. E. Mousavi, J. E. Pask, and N. Sukumar, Efficient adaptive integration of functions with sharp gradients and cusps in n-dimensional parallelepipeds, Int. J. Numer. Methods Eng. **91**, 343 (2012).

[55] F. Sausset and G. Tarjus, Periodic boundary conditions on the pseudosphere, J. Phys. A: Math. Theor. **40**, 12873 (2007).

[56] S. Kirkpatrick, C. D. Gelatt, Jr., and M. P. Vecchi, Optimization by Simulated Annealing, Science **220**, 671 (1983).

[57] F. J. dos Santos, M. dos Santos Dias, F. S. M. Guimarães, J. Bouaziz, and S. Lounis, Spin-resolved inelastic electron scattering by spin waves in noncollinear magnets, Phys. Rev. B **97**, 024431 (2018).

[58] A. Roldán-Molina, M. J. Santander, A. S. Nunez, and J. Fernández-Rossier, Quantum fluctuations stabilize skyrmion textures, Phys. Rev. B **92**, 245436 (2015).

[59] C. Tsallis, Diagonalization methods for the general bilinear Hamiltonian of an assembly of bosons, J. Math. Phys. **19**, 277 (1978).

[60] M.-w. Xiao, Theory of transformation for the diagonalization of quadratic Hamiltonians, arXiv:0908.0787.

[61] K. Mæland, Excitation spectrum and superfluidity of weakly interacting, spin-orbit coupled Bose-Einstein condensate, Master's thesis, Norwegian University of Science and Technology, 2020, https://hdl.handle.net/11250/2785514.

[62] K. Mæland, A. T. G. Janssønn, J. H. Rygh, and A. Sudbø, Plane- and stripe-wave phases of a spin-orbit-coupled Bose-Einstein condensate in an optical lattice with a Zeeman field, Phys. Rev. A **102**, 053318 (2020).